Journal of Magnetic Resonance **141,** 18–28 (1999)
Article ID jmre.1999.1893, available online at http://www.idealibrary.com on IDEAL®

Analysis of Dipolar-Coupling-Mediated Coherence Transfer in a Homonuclear Two Spin-$\frac{1}{2}$ Solid-State System

D. M. Taylor* and A. Ramamoorthy*,†,[1]

*Biophysics Research Division and †Department of Chemistry, The University of Michigan, Ann Arbor, Michigan 48109-1055

Received February 4, 1999; revised July 9, 1999

Homonuclear dipolar-mediated coherence transfer (DCT), a through-space transfer of magnetization between like spins, can yield otherwise difficult-to-obtain structural information for macromolecules by measuring the internuclear distances between two sites of interest. The behavior of a spin-$\frac{1}{2}$ system under DCT is analyzed in detail by computing the time development of the density matrix using the product operator formalism. The effect of coherence transfer (CT) via the homonuclear isotropic scalar coupling on DCT is examined. Analytical and computational results that yield useful information on the frequencies, first-maxima, and first-zero of CT for a uniaxially oriented or a single-crystal solid-state system are presented. The results predict that the evolution of the spin angular momentum operators under the homonuclear dipolar coupling Hamiltonian leads to "cylindrical mixing" unlike "isotropic mixing" due to the strong scalar coupling Hamiltonian. These results will find relevance in both the design of RF pulse sequences for the structural studies of uniaxially oriented biological solids and the interpretation of solution NMR results from proteins embedded in partially oriented bicelles. © 1999 Academic Press

Key Words: **dipolar coupling; scalar coupling; coherence transfer; density matrix; product operators.**

INTRODUCTION

The phenomenon of exchange of nuclear spin magnetization through direct and indirect spin–spin interaction is known as polarization transfer or magnetization transfer or Hartmann–Hahn cross-polarization in NMR spectroscopy (*1*). In this paper, we prefer to use the term "coherence transfer" (CT) to represent this phenomenon as it is a general term which defines the transfer of single-quantum coherence (or magnetization or polarization) and multiple-quantum coherences. CT via the scalar coupling (also known as indirect coupling or through-bond coupling or *J* coupling) is the basic concept behind many successful solution NMR experiments that are routinely used to determine the structure of macromolecules (*1, 2*). On the other hand, in the solid phase, the direct spin–spin interaction (also known as dipolar coupling or through-space interaction) dominates the CT process between nuclei. Indeed, the heteronuclear dipolar coherence transfer is often employed in solid-phase experiments to enhance the sensitivity of low-γ nuclei and/or low natural abundance nuclei (*3*). Generally, homonuclear dipolar-mediated coherence transfer (DCT) cannot be detected in isotropic solutions because random rotational motion of molecules averages out the dipolar couplings, even though incoherent magnetization transfer is still possible, resulting in efficient relaxation (*2*). In most static solids, except uniaxially oriented solids, overlap of broad spectral lines complicates the study of DCT.

In magic-angle spinning experiments, selective recovery of the homonuclear spin-$\frac{1}{2}$ dipolar coupling and the measurement of coherent homonuclear DCT is possible using specific pulse sequences (*4–37*). The strong distance dependence of DCT makes the quantification of this effect attractive for use as a distance measurement tool. An understanding of these exchange modes can aid in the design of multiple-pulse sequences to assure the greatest transfer of coherence from a specific spin at a certain experimental time. In fact, solid-state NMR techniques designed based on the concept of DCT are routinely used to provide interatomic distance information in macromolecules (samples excepting isotropic liquids), such as crystalline polymers, liquid crystals, fibrous biopolymers, peptides or proteins in cell membranes, and other biological solids (*38–54*).

Further experimental design of pulse sequences requires a theoretical treatment of DCT in various systems, which must be laid as a groundwork for more complex collection of spins. Because of the nature of the dipolar interaction between like spins, analytical solutions to homonuclear coherence transfer prove to be complex even for simple two-spin systems. Previous publications have done much to clarify the strong and weak coupling effects on the spectral features of homonuclear spin-$\frac{1}{2}$ dipolar-coupled systems (*22, 23*). In this paper, we will employ theoretical tools to explore the modes of homonuclear DCT in a uniaxially oriented or single-crystal solid-state system, consisting of two spin-$\frac{1}{2}$ homonuclei.

THEORY

Consider a two chemically inequivalent homonuclear spin-$\frac{1}{2}$ nuclei in a uniaxially oriented or a single-crystal sample. We assume that the dipolar coupling as well as the scalar coupling

[1] To whom correspondence should be addressed. Fax: (734) 764-8776. E-mail: ramamoor@umich.edu.

1090-7807/99 $30.00
Copyright © 1999 by Academic Press
All rights of reproduction in any form reserved.

TABLE 1
Evolution of Spin Operators under the Coupling Hamiltonian, H_{JD}

	Operators generated after evolution under H_{JD}											
Initial state	I_x	S_x	I_y	S_y	I_z	S_z	$2I_xS_z$	$2I_zS_x$	$2I_yS_z$	$2I_zS_y$	$2I_xS_y$	$2I_yS_x$
I_x	A	B							−E	F		
S_x	B	A							F	−E		
I_y			A	B			E	−F				
S_y			B	A			−F	E				
I_z					C	D					−G	G
S_z					D	C					G	−G
$2I_xS_z$			−E	F			A	−B				
$2I_zS_x$			F	−E			−B	A				
$2I_yS_z$	E	−F							A	−B		
$2I_zS_y$	−F	E							−B	A		
$2I_xS_y$					G	−G					C	D
$2I_yS_x$					−G	G					D	C

Note. The expectation values of the spin operators are given.

between the two nuclei is nonzero. Further, relaxation effects are ignored in the present theoretical study. The total Hamiltonian for this system in the presence of a static external magnetic field consists of chemical shift, scalar coupling, and dipolar coupling terms.

$$H_T = H_D + H_{CS} + H_J \qquad [1]$$

We assume that an experimental situation can be created to selectively suppress the chemical shift interaction with minimal or no effect on the coupling terms of the total Hamiltonian H_T. Then the total Hamiltonian in Eq. [1] becomes the sum of H_D and H_J. Henceforth, we refer to this total Hamiltonian (H_T) as the coupling Hamiltonian (H_{JD}); $H_T = H_D + H_J = H_{JD}$. This Hamiltonian is equivalent to the creation of a zero-field or rotating-frame Hamiltonian in a solid-state NMR experiment. A simple spin echo sequence, in the form of a series of 180° pulses, can be used to refocus the chemical shifts and leave the scalar as well as the dipolar couplings unaltered. On the other hand, a multiple RF pulse sequence can be used to spin lock as well as scale the homonuclear dipolar coupling. For example, consider a multiple RF pulse sequence consisting of a spin echo sequence for one half of the cycle and magic echo sequence for the second half of the cycle. It can be shown using the average Hamiltonian theory that the effective Hamiltonian of this unified spin echo and magic echo (USEME) (*17*) pulse sequence is $0.5\,H_D + H_J$. The spin echo sequence, consisting of a series of π pulses, suppresses the chemical shift interaction and leaves the dipolar and scalar couplings unaltered. On the other hand, the magic echo sequence suppresses the chemical shift interaction, scales the dipolar coupling interaction by a factor of -0.5, and leaves the scalar couplings unaltered. Thus, a complete cycle of USEME suppresses the chemical shift interaction, scales the dipolar coupling interaction by a factor of $+0.5$, and leaves the scalar couplings unaltered. Therefore, a solid-state NMR experiment can be designed to study the coherence transfer between two coupled (dipolar as well as scalar) spin-$\frac{1}{2}$ nuclei in a uniaxially oriented or a single-crystal system. Such a study will be useful in measuring the orientation of the chemical bond or a peptide plane in order to determine the backbone conformation of polypeptides embedded in phospholipid bilayers. For example, the coupling $^{13}C_\alpha$–^{13}CO parameter can be measured on uniaxially oriented biological solids.

In this paper, coherence transfer modes are analyzed under the total coupling Hamiltonian, H_{JD}. In static solids, usually the scalar coupling term, H_J, is smaller in magnitude than the dipolar coupling term and is often neglected. The scalar coupling becomes important in oriented solid-phase samples especially when the homonuclear dipolar coupling is small. Therefore, the effect of the scalar coupling on CT via the dipolar coupling is included in our calculations. The dipolar coupling Hamiltonian can be expressed in the form of spherical tensors,

TABLE 2
Coefficients of the Spin Operators Generated Due to the Evolution under H_{JD} and Their First-Maxima and First-Zero

Coefficients of spin operators	Figure	First-maxima	First-zero
$A = 0.5(\cos \alpha\pi t + \cos \beta\pi t)$	1a	$-4/D_{IS}$	$-1/(2D_{IS})$
$B = 0.5(-\cos \alpha\pi t + \cos \beta\pi t)$	1b	[a]	$-1/D_{IS}$
$C = 0.5(1 + \cos \gamma\pi t)$	1c	$-2/D_{IS}$	$-1/D_{IS}$
$D = 0.5(1 - \cos \gamma\pi t)$	1d	$-1/D_{IS}$	$-2/D_{IS}$
$E = 0.5(\sin \alpha\pi t + \sin \beta\pi t)$	1e	[a]	$-1/D_{IS}$
$F = 0.5(\sin \alpha\pi t - \sin \beta\pi t)$	1f	$-3/D_{IS}$	$-1/(2D_{IS})$
$G = 0.5(\sin \gamma\pi t)$	1g	$-1/(2D_{IS})$	$-1/D_{IS}$

Note. [a] No analytical solution was found. $\alpha = (D_{IS}/2 + J)$; $\beta = (3D_{IS}/2)$; $\gamma = (J - D_{IS})$; $D_{IS} = -\hbar\gamma_I\gamma_S/2\pi r_{IS}^3$.

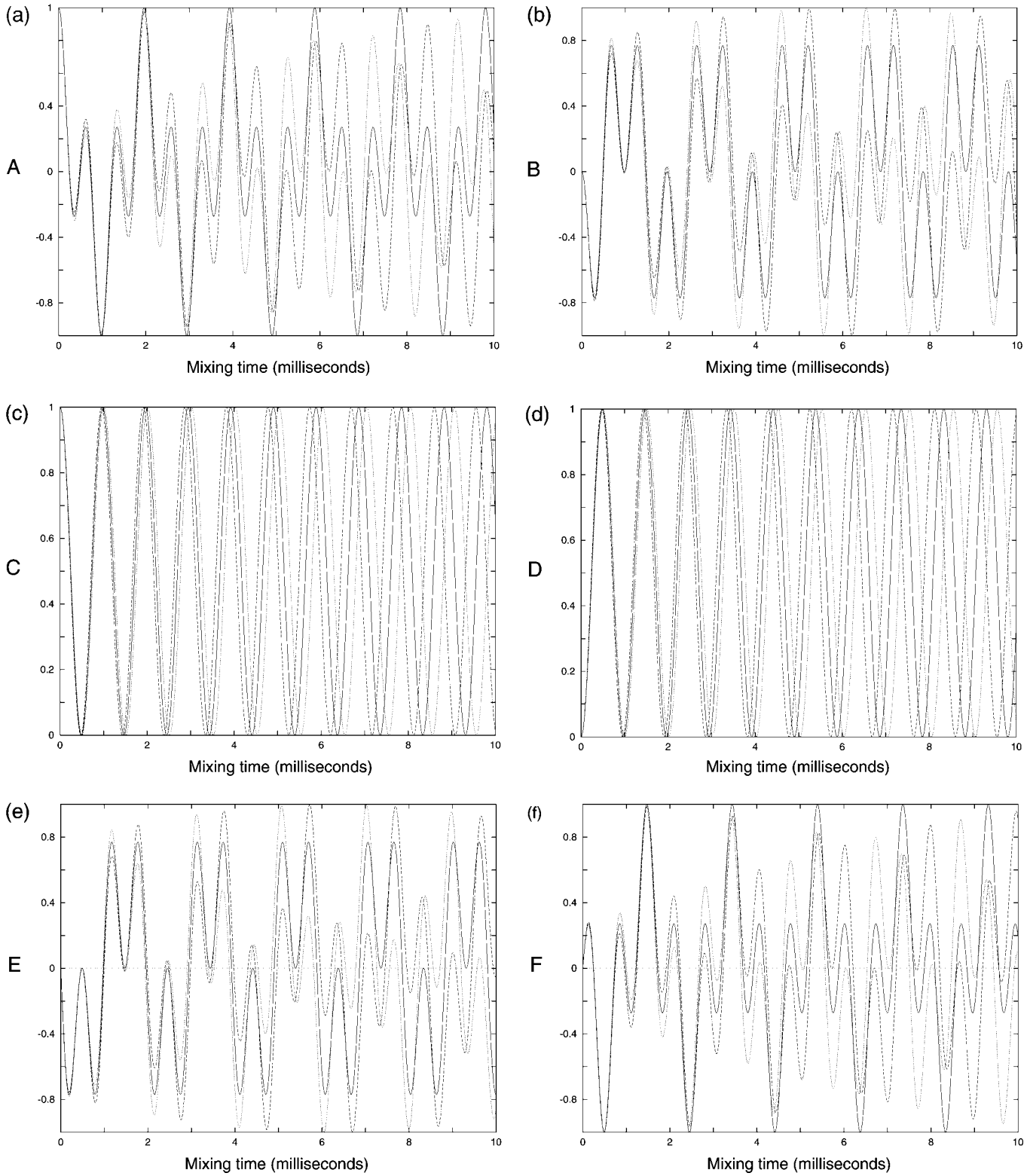

FIG. 1. Expectation values of various spin operators under the dipolar coupling Hamiltonian, H_D (solid lines), and the total coupling Hamiltonian, H_{JD} (dotted and dashed lines). The coefficients of the spin operators given in Table 1 are plotted as a function of evoluition time in an oriented or single-crystal system containing two ^{13}C nuclei separated by a distance of 1.55 Å. The dotted lines are for $J = -53$ Hz and the dashed lines are for $J = 53$ Hz. For example, in (a), the magnitude of the term A is plotted as a function of the evolution time under the Hamiltonian H_{JD}. This can be used to evaluate the amount of magnetization which remains in the source or in I nuclei when x magnetization of the I nuclei is selected for the coherence transfer under the coupling Hamiltonian. Similarly, in (b), the magnitude of the term B is plotted as a function of the evolution time under the Hamiltonian H_{JD}. This can be used to evaluate the amount of magnetization transferred to the S nuclei when x magnetization of the I nuclei is selected for the coherence transfer under the coupling Hamiltonian.

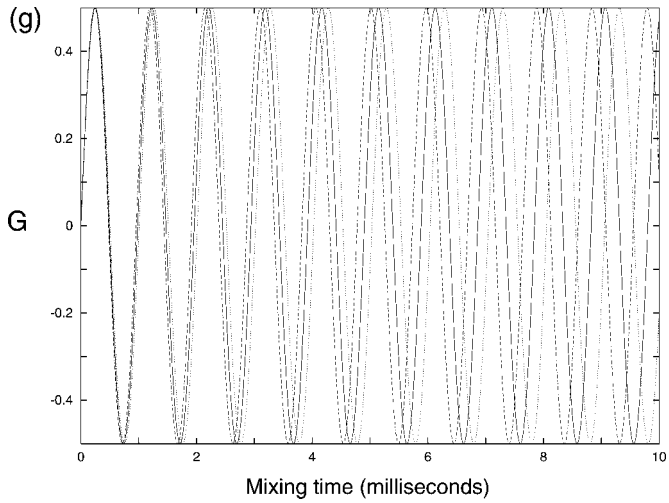

FIG. 1—*Continued*

$$H_D = \sum_{q=-2}^{+2} (-1)^q D_{2q} T_{2-q}, \qquad [2]$$

where the second-rank tensors D_{2q} and T_{2-q} define the spatial and spin parts of the dipolar coupling Hamiltonian (*55*). The secular dipolar coupling Hamiltonian can be given as (*55*)

$$H_D = \frac{\hbar \gamma_I \gamma_S}{4\pi r_{IS}^3} [1 - 3\cos^2\theta](3I_zS_z - I \cdot S), \qquad [3]$$

where θ is the angle between the magnetic field and the vector connecting the two spins, r_{IS} is the distance between I and S nuclei, and γ_i is the gyromagnetic ratio of nucleus i. Since the structure of the direct and indirect coupling Hamiltonians for a homonuclear spin system is similar, the total coupling Hamiltonian is given as

$$H_{JD} = (2D_{IS} + J)I_zS_z - (D_{IS} + J)\{I_xS_x + I_yS_y\}, \qquad [4]$$

where J is the scalar coupling constant and D_{IS} is the dipolar coupling frequency defined as

$$D_{IS} = \frac{\hbar \gamma_I \gamma_S}{4\pi r_{IS}^3} [1 - 3\cos^2\theta]. \qquad [5]$$

In order to evaluate the coherence transfer modes due to the evolution under the coupling Hamiltonian, we assume a uniaxially oriented system with $\theta = 0°$. Any change in the value of θ will only change the magnitude of the D_{IS} parameter.

RESULTS AND DISCUSSION

The evolution of all the spin operators that span the two-spin space under the coupling (both scalar and dipolar) Hamiltonian (see Eq. [4]) is evaluated and the results are summarized in Tables 1 and 2. The spin part of the total coupling Hamiltonian, H_{JD}, is composed of a term I_zS_z, identical to the weak scalar coupling Hamiltonian, and a term $I \cdot S$, identical to the strong scalar coupling Hamiltonian. Since these two terms commute, the evolutions under both these terms were sequentially carried out in the calculations. Further, the calculations are simplified because the product operators in $I \cdot S$ commute with each other. Since the operators I_zS_z, I_yS_y, and I_xS_x commute with H_{JD}, they have a constant of motion under H_{JD}, and therefore they are not given in Table 1. In other words, the expectation values of the spin operators are summarized in Table 1 for an evolution of a two homonuclear spin-$\frac{1}{2}$ system under the coupling Hamiltonian H_{JD}.

An initial state of the spin system is specified in the first column of Table 1 and the coefficients of the product operators in the final density matrix are given in the subsequent columns of Table 1. For example, the evolution of the initial density matrix representing the x magnetization of the nuclei I, the I_x operator, under H_{JD} is given as

$$\begin{aligned} I_x \xrightarrow{H_{JD}} & \tfrac{1}{2}(\cos\alpha\pi t + \cos\beta\pi t)I_x \\ & + (\cos\beta\pi t - \cos\alpha\pi t)S_x \\ & + \tfrac{1}{2}(1 + \cos\gamma\pi t)2I_yS_z \\ & + \tfrac{1}{2}(1 - \cos\gamma\pi t)2I_zS_y. \end{aligned} \qquad [6]$$

The angles α, β, and γ are defined in Table 2. This equation can be realized by reading across the row of Table 1. This corresponds to the selective preparation of the x magnetization of the I nuclear spins and allowing an evolution under a specifically designed RF pulse sequence that leaves the coupling Hamiltonian unaltered in an experiment. It is clear from Eq. [6] that the evolution of the I_x operator under H_{JD} leads to I_x, S_x, I_yS_z, and I_zS_y operators. In other words, the observable x magnetization of I nuclear spin (or I_x) is transferred as the observable x magnetization of S nuclear spin (or S_x), as well as antiphase I (or I_yS_z) and S (or I_zS_y) magnetizations. The expectation values of I_x, S_x, I_yS_z, and I_zS_y operators for the evolution of the I_x operator under the Hamiltonian H_{JD} is given by the terms A, B, $-$E, and F, respectively.

The coefficients of the product operators are plotted as a function of the evolution time in Fig. 1 for a ^{13}C–^{13}C system with a dipolar coupling $D_{CC} = -2038$ Hz corresponding to a distance $r_{CC} = 1.55$ Å. These data represent the distance and the dipolar coupling between the directly bonded $^{13}C_\alpha$ and ^{13}CO nuclei in the backbone of a peptide. Analysis of the Fourier transform of these time-domain functions yields spectra that consist of dipolar as well as scalar coupling information.

In Fig. 1, the evolution of spin operators is represented in solid, dotted, and dashed lines for $J = 0$, $J = -53$, and $J =$

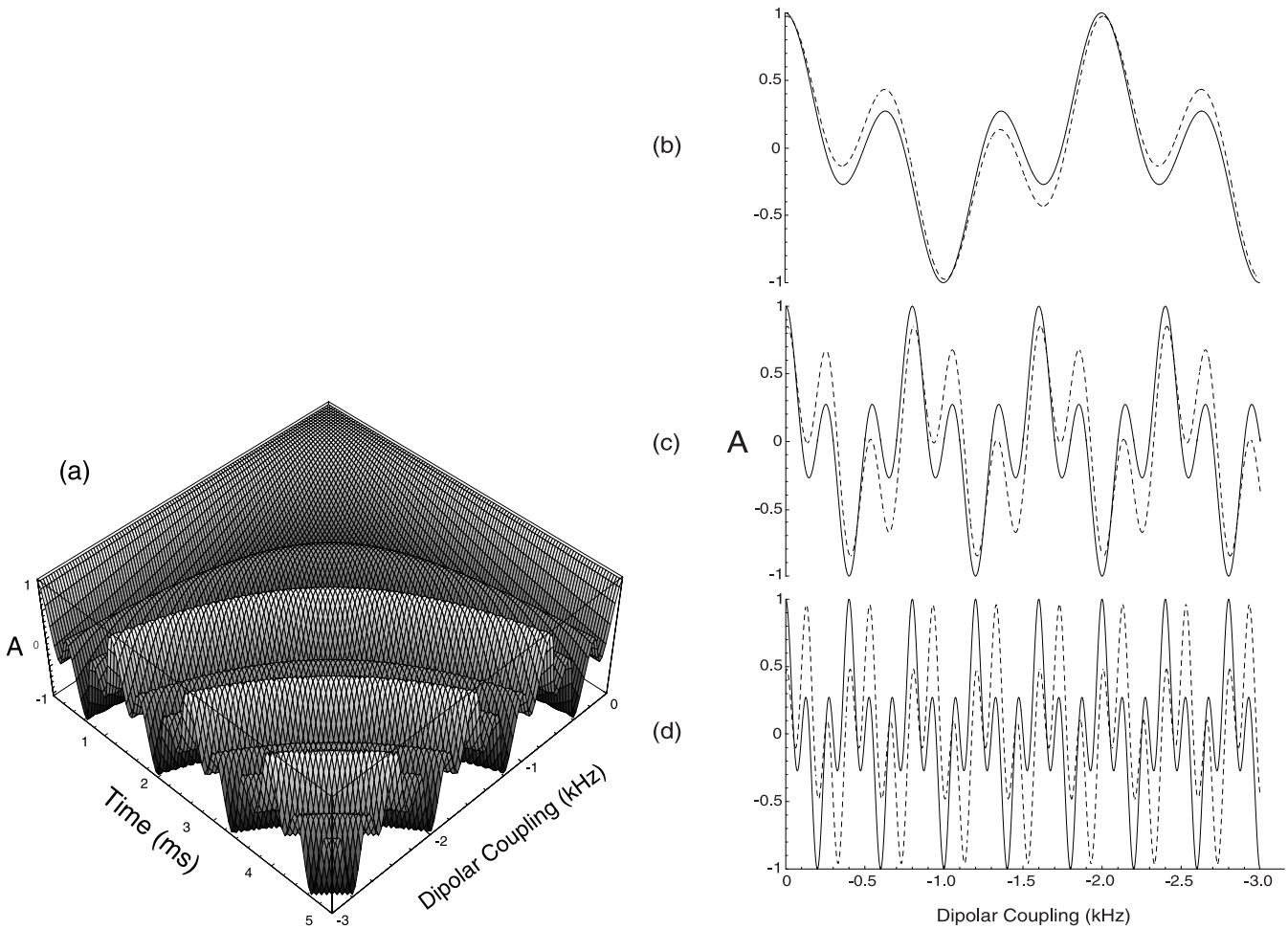

FIG. 2. (a) Three-dimensional plot showing the dependence of the expectation value of the I_x operator during the evolution of the I_x operator under the H_D Hamiltonian (as given by the term A in Table 1) on the dipolar coupling and the evolution time. Two-dimensional slices (b), (c), and (d) taken from the three-dimensional plot in (a) for the evolution times 2, 5, and 10 ms, respectively, are shown for $J = 0$ (solid lines) and for $J = 53$ Hz (dashed lines).

53 Hz, respectively. For example, in Fig. 1a, the magnitude of the term A is plotted as a function of the evolution time under the Hamiltonian H_{JD}. This function can be used to evaluate the amount of magnetization that remains in the source (or in the I nuclei) when the x magnetization of the I nuclei is selected for the coherence transfer under the coupling Hamiltonian H_{JD}. Similarly, in Fig. 1b, the magnitude of the term B is plotted as a function of the evolution time under the Hamiltonian H_{JD}. This function can be used to evaluate the amount of magnetization transferred to the S nuclei when x magnetization of the I nuclei is selected for the coherence transfer under the coupling Hamiltonian H_{JD}.

The evolution of spin operators under any one of the coupling Hamiltonians (H_D or H_J) can easily be separated using the results from Tables 1 and 2. It can be seen from Eq. [6] that the dipolar coupling Hamiltonian leads to *in-phase* as well as *antiphase* transfer of magnetization like the scalar coupling Hamiltonian. The *in-phase* transfer of x magnetization can be understood from Figs. 1a and 1b. Even though the transfer of a transverse magnetization via H_D and H_J appears to be similar, the evolution frequencies of the spin operators are different for both cases. In the case of the H_J mixing Hamiltonian, the active frequencies in the evolution are the same, that is, πJ, for all spin operators. But in the case of the H_D mixing Hamiltonian, the evolution frequencies are a combination of two different frequency terms, $0.5\ \pi D_{IS}$ and $1.5\ \pi D_{IS}$, for all spin operators as seen from the expressions for A, B, E, and F in Table 2. It may be noted that the evolutions of x and y magnetizations under the total coupling Hamiltonian H_{JD} or under the individual coupling Hamiltonians (H_D or H_J) are similar as seen from Tables 1 and 2 and Fig. 1.

As shown in Table 1 and Fig. 1, the evolution of *antiphase* product operators, I_pS_q and I_qS_p ($p = x$ or y; $q = z$), is similar to that of I_p ($p = x$ or y) operators. They lead to *in-phase* x or y magnetization in addition to *antiphase* product operators. This suggests that the antiphase multiplet signal can be refocused into an *in-phase* multiplet for detection just like RINEPT experiments (*1*) for a weakly scalar coupled spin

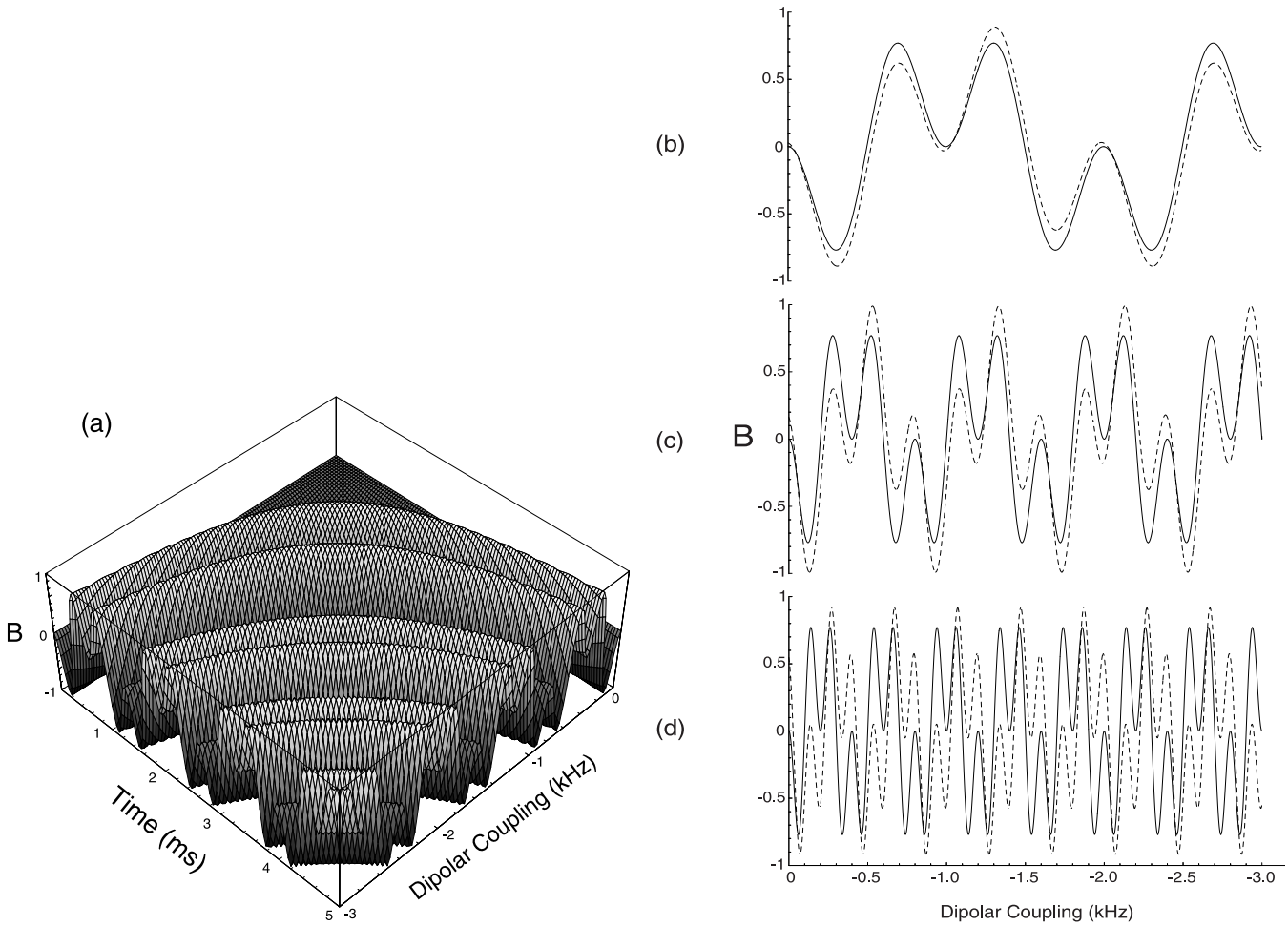

FIG. 3. (a) Three-dimensional plot showing the dependence of the expectation value of the S_x operator during the evolution of the I_x operator under the H_D Hamiltonian (as given by the term B in Table 1) on the dipolar coupling and the evolution time. Two-dimensional slices (b), (c), and (d) taken from the three-dimensional plot in (a) for the evolution times 2, 5, and 10 ms, respectively, are shown for $J = 0$ (solid lines) and for $J = 53$ Hz (dashed lines).

system in isotropic solutions. This strategy will be highly valuable as the broad lines of the antiphase doublet in solids will be difficult to observe, especially when the dipolar coupling is small. The evolution times under the coupling Hamiltonian for the maximum conversion of I_x into I_zS_y, S_x into I_yS_z, I_y into $-I_zS_x$, S_y into $-I_xS_z$, I_zS_y into $-I_x$, I_yS_z into $-S_y$, I_zS_x into I_y, and I_xS_z into S_y are the same as given by the term F in Fig. 1f.

The evolution of the I_z (or S_z) operator under H_D is significantly different from that of the transverse components, I_x (or S_x) and I_y (or S_y), unlike the case of H_J as can be seen from Tables 1 and 2 and Fig. 1. This is mainly because the spin part of the dipolar coupling Hamiltonian that is operative on these angular momentum operators is different. They are $3I_zS_z - I_yS_y$ for I_x (or S_x), $3I_zS_z - I_xS_x$ for I_y (or S_y), and $-I_xS_x - I_yS_y$ for I_z (or S_z) since $[I_i, I_iS_i] = 0$ and $[S_i, I_iS_i] = 0$. For the evolution of the I_z (or S_z) operator under H_{JD}, the frequency of evolution of the spin operators in the final density matrix is $\pi(J - D)$. In fact, the transfer of z magnetization via H_D, H_J, and H_{JD} is similar. They all yield an observable *in-phase* coherence transfer as well as an unobservable zero-quantum coherence (ZQC), $I_xS_y - I_yS_x$. The only difference is the rate of coherence transfer. It is also to be noted that the evolution of the ZQC under the coupling Hamiltonians H_D, H_J, and H_{JD} is similar. They all yield an observable z magnetization (see Table 1) but the only difference is the rate of coherence transfer. Therefore, any solution NMR methods that employ mixing of z magnetization or ZQC via the isotropic scalar coupling can either be adapted or suitably modified, depending on the strength of the homonuclear dipolar coupling, for solid-state NMR studies on uniaxially oriented systems (*56–58*).

Although the structure of H_J and H_D Hamiltonians is similar, there is a significant difference between the coherence transfer via the scalar and the dipolar couplings. This is because the contribution to the CT process from the z component is different from that of the x and y components of the dipolar coupling Hamiltonian H_D unlike the case of the strong scalar coupling Hamiltonian H_J. In other words, evolution of the spin angular momentum operators under the strong scalar coupling

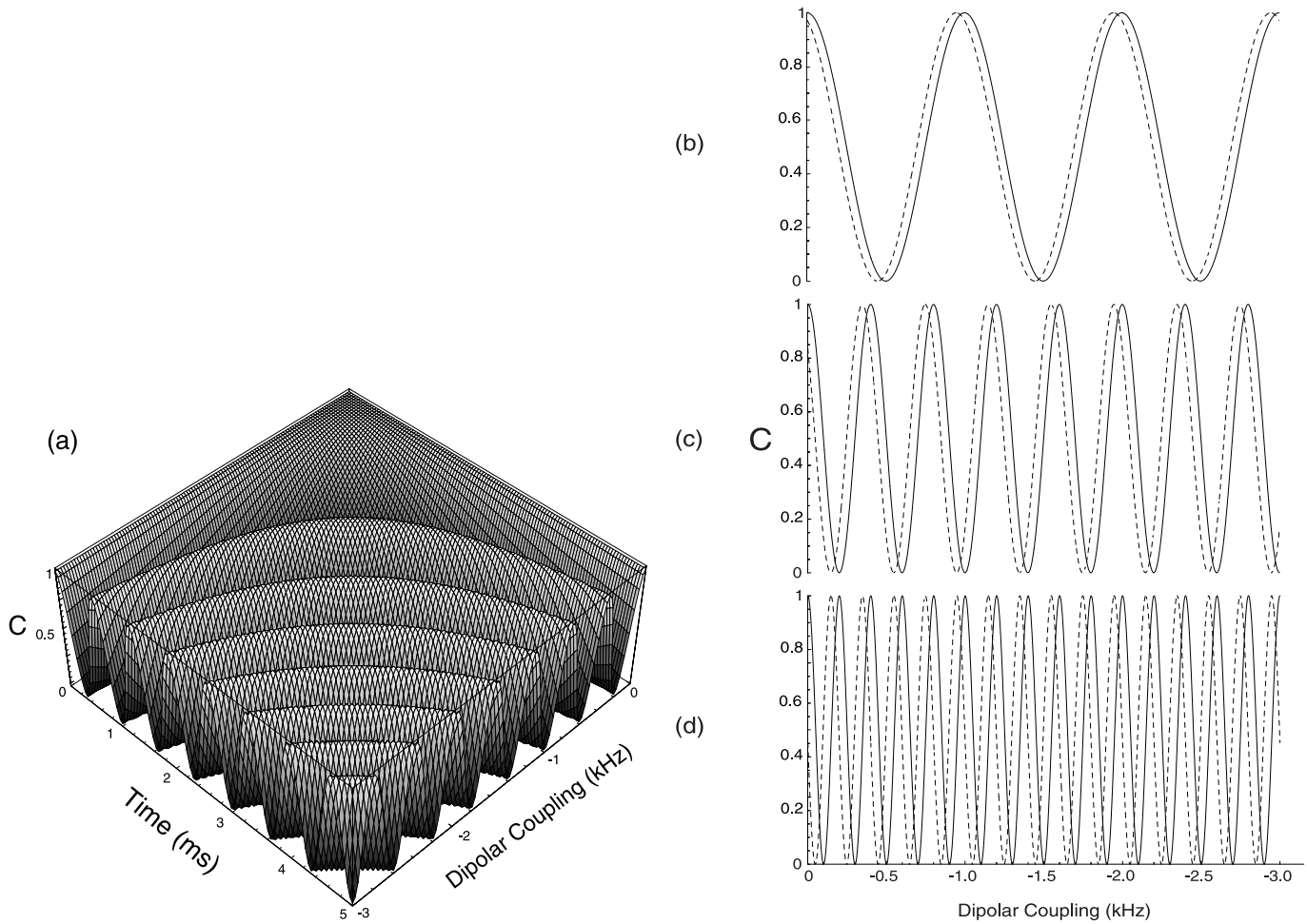

FIG. 4. (a) Three-dimensional plot showing the dependence of the expectation value of the I_z operator during the evolution of the I_z operator under the H_{JD} Hamiltonian (as given by the term C in Table 1) on the dipolar coupling and the evolution time. Two-dimensional slices (b), (c), and (d) taken from the three-dimensional plot in (a) for the evolution times 2, 5, and 10 ms, respectively, are shown for $J = 0$ (solid lines) and for $J = 53$ Hz (dashed lines).

Hamiltonian H_J leads to *isotropic mixing*, that is, all three components of the Hamiltonian H_J are equally operative, while evolution under the dipolar coupling Hamiltonian H_D leads to *cylindrical mixing*, that is, only two of the three components of the Hamiltonian H_D are equally operative. Therefore, the homonuclear dipolar coupling Hamiltonian H_D may be termed a cylindrical mixing Hamiltonian in analogy to the name isotropic mixing Hamiltonian for the strong scalar coupling Hamiltonian H_J. It is also to be noted that the term $I_i + S_i$ ($i = x$, y, z) has a constant of motion under H_J while only the term $I_z + S_z$ has a constant of motion under H_D. This suggests that a nonselectively prepared transverse magnetization in an experiment evolves under the influence of the dipolar coupling but not under the scalar coupling. It is interesting to note that a pair of chemically equivalent nuclei also evolves under the dipolar coupling during a spin-locking RF field as the I_zS_z term of H_D does not commute with the RF Hamiltonian, unlike in the case of scalar coupling.

The three-dimensional plot in Fig. 2a shows the dependence of the term A on the dipolar coupling frequency and the evolution time during the evolution of the spin system under the H_{JD} Hamiltonian. Two-dimensional slices in Figs. 2b to 2d are taken from the three-dimensional plot in Fig. 2a for various evolution times, while varying the dipolar coupling from 0 to -3 kHz. The dependence of the terms B, C, and D on the dipolar coupling and the evolution time are presented in Figs. 3, 4, and 5, respectively. It is evident from the two-dimensional plots (see Figs. 2–5) that the number of maxima of the terms A, B, C, and D against the dipolar coupling increases as a function of the evolution time. For example, in Fig. 2a, for an evolution time of 2 ms under a dipolar coupling of about -2 kHz, the transfer of x magnetization of the I nuclei to its dipolar coupled partner is zero as can be seen from Figs. 2b and 3b. On the other hand, the maximum transfer occurs at a dipolar coupling of about -0.65 kHz (see Fig. 3b). It is interesting that I_x is transferred as $\pm S_x$ depending on the magnitude of dipolar coupling and the evolution time. Therefore, care must be taken in quantifying the degree of DCT. The effect of the scalar coupling, $J = 53$ Hz, is shown in dashed lines in Figs. 2–5. As the mixing time increases, the CT process is significantly

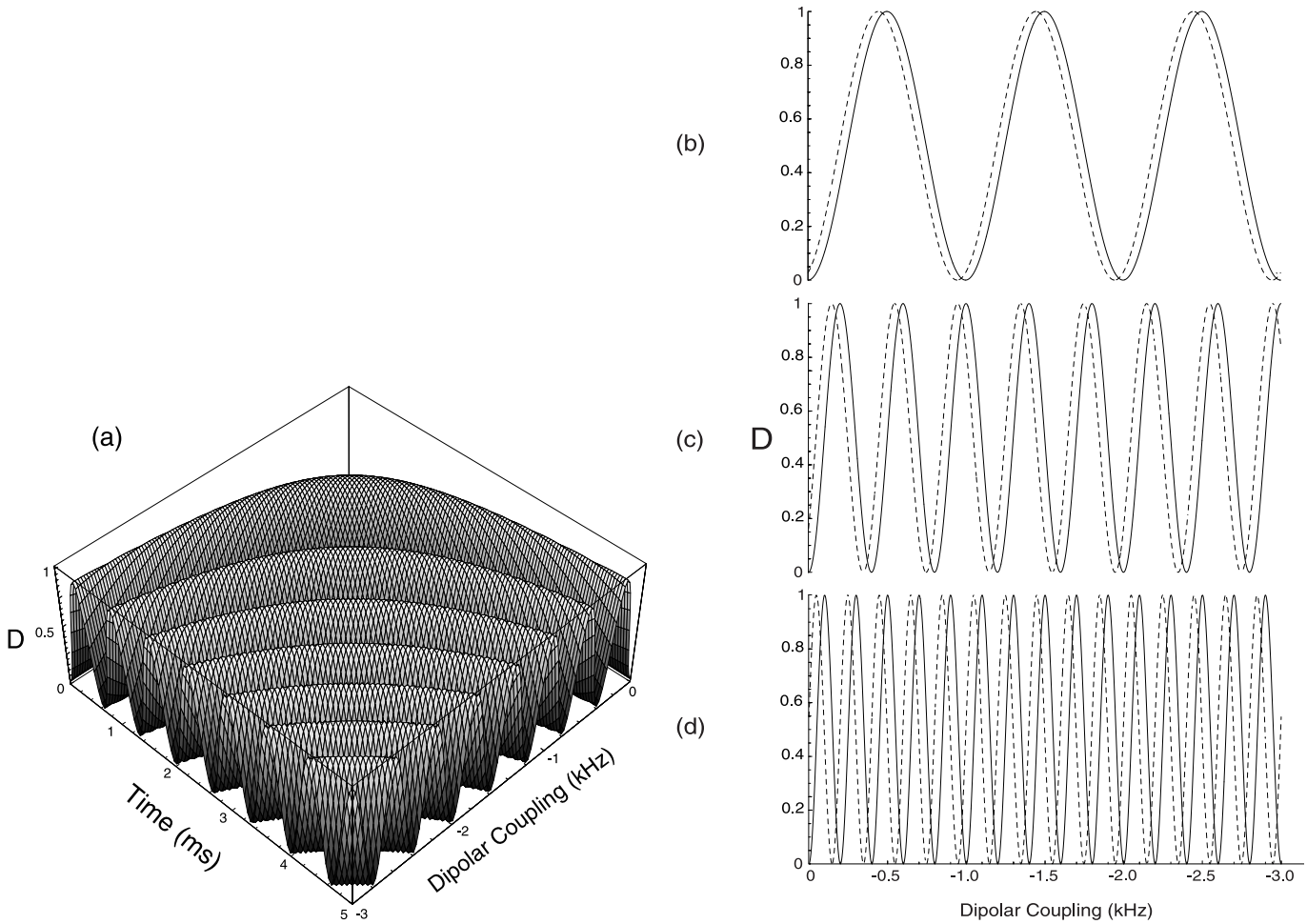

FIG. 5. (a) Three-dimensional plot showing the dependence of the expectation value of the S_z operator during the evolution of the I_z operator under the H_{JD} Hamiltonian (as given by the term D in Table 1) on the dipolar coupling and the evolution time. Two-dimensional slices (b), (c), and (d) taken from the three-dimensional plot in (a) for the evolution times 2, 5, and 10 ms, respectively, are shown for $J = 0$ (solid lines) and for $J = 53$ Hz (dashed lines).

dependent on the J parameter as evident from Figs. 2d, 3d, 4d, and 5d.

First-maxima and first-zero of the coefficients of the spin operators are given in Table 2. The functions with no simple analytical solution for maxima are noted in the table. A nonzero scalar coupling not only changes the coherence transfer efficacy as indicated in Fig. 1 but also shifts the first-maxima and first-zero of the functions in Table 2. The presence of J makes it difficult to obtain an analytical solution for the first-maxima and first-zero for the CT process. Further, it is important to note that the absolute sign of J coupling changes the CT process as shown in Fig. 1. These effects become significant if the dipolar coupling becomes smaller due to either the partial averaging of the dipolar coupling or the orientation of the dipole–dipole vector near the magic angle. Therefore care must be taken in the experimental measurement of small dipolar couplings in order to obtain accurate interatomic distances. The dependence of the terms A, B, C, and D on the ratio of the scalar and dipolar couplings and on the evolution time is presented in Fig. 6. The results suggests that even small differences in the ratio of the couplings can make a significant difference in the CT efficacy.

CONCLUSIONS

Coherence transfer under the dipolar coupling between a homonuclear spin-$\frac{1}{2}$ pair and the effects of the scalar coupling on DCT are analyzed in detail. The results suggest that DCT is a cylindrical mixing process unlike the isotropic mixing process under the strong scalar coupling Hamiltonian. The simple forms of the analytical equations that describe the coherence transfer under the dipolar coupling avail themselves to quick numerical simulations for experiments on oriented solid-state systems. It is clear that even small values of J compared to the dipolar coupling can make significant changes in the coherence transfer efficacy, and therefore the effect of J must be considered for the design of pulse sequences for the interatomic distance measurements and also to interpret the data from an oriented system, especially when the dipolar coupling is small. This may be significant in the study of partially oriented

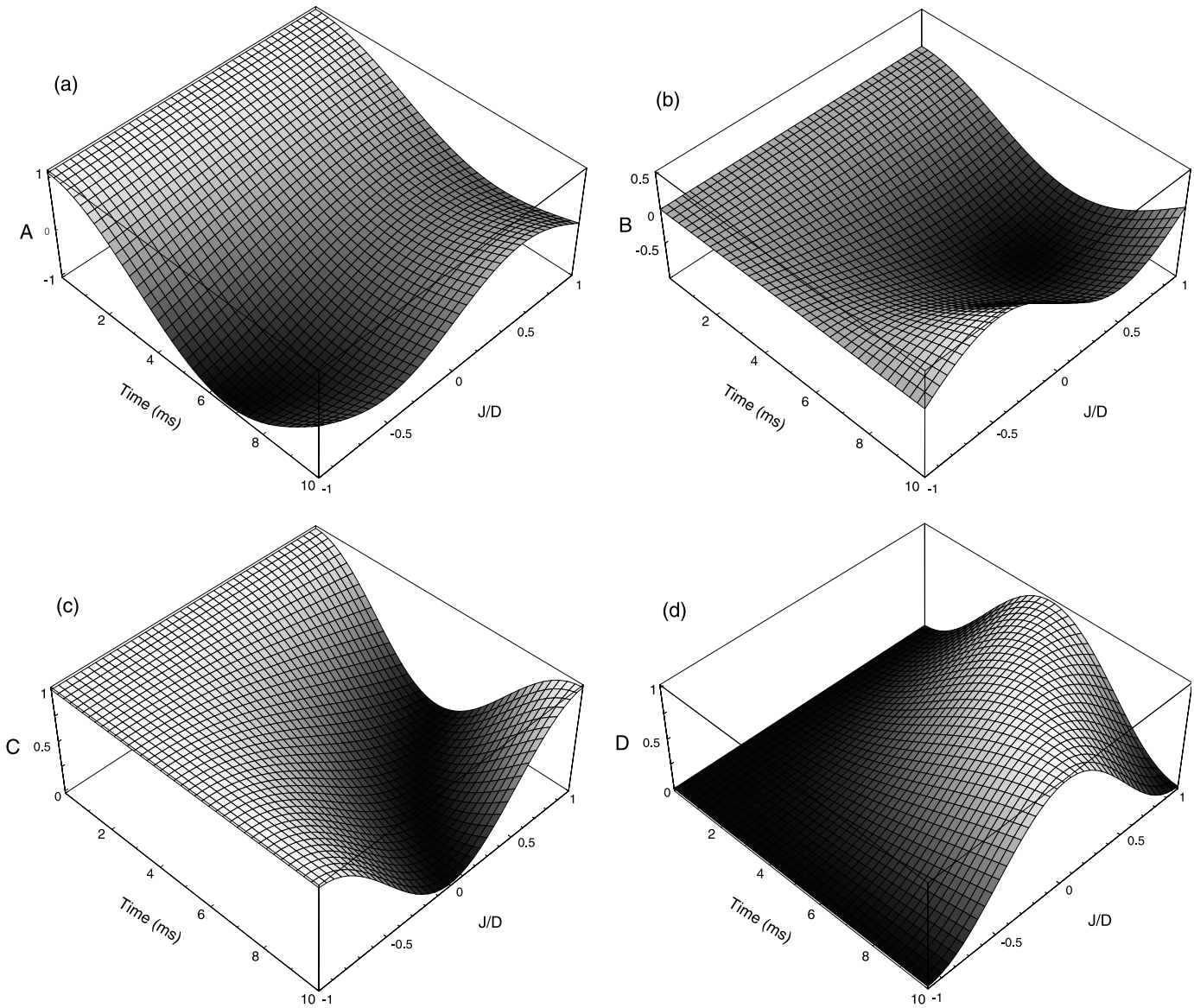

FIG. 6. Three-dimensional plots showing the dependence of the terms A, B, C, and D on the ratio of the scalar and dipolar couplings are shown in (a), (b), (c), and (d), respectively. The dipolar coupling was assumed to be 100 Hz.

bicelles that are currently used to obtain large interatomic distance constraints for the structure determination of globular proteins using solution NMR methods (*59–61*). Furthermore, the results from this work will be useful for designing experiments based on DCT, especially for the structural studies of uniaxially oriented biological solids (*56–58*), in solid-state NMR spectroscopy.

ACKNOWLEDGMENTS

Acknowledgment is made to the donors of the Petroleum Research Fund, administered by the American Chemical Society, for partial support of this research. D. M. Taylor acknowledges the Center for the Education of Women at the University of Michigan for the Margaret Dow Towsley Scholarship and for the Sloan Summer Fellowship.

REFERENCES

1. R. R. Ernst, G. Bodenhausen, and A. Wokaun, "Principles of Nuclear Magnetic Resonance in One and Two Dimensions," Sections 2.1.11 and 4.5, Clarendon Press, Oxford (1987).
2. K. Wuthrich, "NMR of Proteins and Nucleic Acids," Wiley–Interscience, New York (1986).
3. A. Pines, M. G. Gibby, and J. S. Waugh, Proton-enhanced NMR of dilute spins in solids, *J. Chem. Phys.* **59,** 569–590 (1973).
4. B. H. Meier and W. L. Earl, Excitation of multiple quantum transitions under magic angle spinning conditions: Adamantane, *J. Chem. Phys.* **85,** 4905–4911 (1986).
5. B. H. Meier and W. L. Earl, A double-quantum filter for rotating solids, *J. Am. Chem. Soc.* **109,** 7937–7942 (1987).
6. D. P. Raleigh, M. H. Levitt, and R. G. Griffin, Rotational resonance in solid state NMR, *Chem. Phys. Lett.* **146,** 71–76 (1988).

7. M. G. Colombo, B. H. Meier, and R. R. Ernst, Rotor-driven spin diffusion in natural-abundance ^{13}C spin systems, *Chem. Phys. Lett.* **146,** 189–196 (1988).
8. M. H. Levitt, T. G. Oas, and R. G. Griffin, Rotary resonance recoupling in heteronuclear spin pair systems, *Isr. J. Chem.* **28,** 271–282 (1988).
9. P. Robyr, B. H. Meier, and R. R. Ernst, Radio-frequency-driven nuclear spin diffusion in solids, *Chem. Phys. Lett.* **162,** 417–423 (1989).
10. M. H. Levitt, D. P. Raleigh, F. Creuzet, and R. G. Griffin, Theory and simulation of homonuclear spin pair systems in rotating solids, *J. Chem. Phys.* **92,** 6347–6364 (1990).
11. Z. H. Gan and D. M. Grant, Rotational resonance in a spin-lock field for solid state NMR, *Chem. Phys. Lett.* **168,** 304–308 (1990).
12. R. Tycko and G. Dabbagh, Measurement of nuclear magnetic dipole–dipole couplings in magic angle spinning NMR, *Chem. Phys. Lett.* **173,** 461–465 (1990).
13. A. E. Bennett, J. H. Ok, R. G. Griffin, and S. Vega, Chemical shift correlation spectroscopy in rotating solids: Radio frequency-driven dipolar recoupling and longitudinal exchange, *J. Chem. Phys.* **96,** 8624–8627 (1992).
14. J. H. Ok, R. G. S. Spencer, A. E. Bennett, and R. G. Griffin, Homonuclear correlation spectroscopy in rotating solids, *Chem. Phys. Lett.* **197,** 389–396 (1992).
15. N. C. Nielsen, F. Creuzet, R. G. Griffin, and M. H. Levitt, Enhanced double-quantum nuclear magnetic resonance in spinning solids at rotational resonance, *J. Chem. Phys.* **96,** 5668–5677 (1992).
16. T. Gullion and S. Vega, A simple magic angle spinning NMR experiment for the dephasing of rotational echoes of dipolar coupled homonuclear spin pairs, *Chem. Phys. Lett.* **194,** 423–428 (1992).
17. T. Fujiwara, A. Ramamoorthy, K. Nagayama, K. Hioka, and T. Fujito, Dipolar HOHAHA under MAS conditions for solid-state NMR, *Chem. Phys. Lett.* **212,** 81–84 (1993).
18. R. Tycko and S. O. Smith, Symmetry principles in the design of pulse sequences for structural measurements in magic angle spinning nuclear magnetic resonance, *J. Chem. Phys.* **98,** 932–943 (1993).
19. D. K. Sodickson, M. H. Levitt, S. Vega, and R. G. Griffin, Broad band dipolar recoupling in the nuclear magnetic resonance of rotating solids, *J. Chem. Phys.* **98,** 6742–6748 (1993).
20. N. C. Nielsen, F. Creuzet, and R. G. Griffin, Rotationally enhanced exchange of Zeeman order via two-dimensional switched-speed spinning NMR, *J. Magn. Reson. A* **103,** 245–252 (1993).
21. R. G. S. Spencer, K. W. Fishbein, M. H. Levitt, and R. G. Griffin, Rotational resonance with multiple-pulse scaling in solid-state nuclear-magnetic-resonance, *J. Chem. Phys.* **100,** 5533–5545 (1994).
22. T. Nakai and C. A. McDowell, Residual chemical-shift effects in spin-echo NMR powder patterns of homonuclear dipolar-coupled spins, *Chem. Phys. Lett.* **217,** 234–238 (1994).
23. T. Nakai and C. A. McDowell, Characterization of homonuclear spin pairs from two-dimensional spin-echo NMR powder patterns, *J. Am. Chem. Soc.* **116,** 6373–6383 (1994).
24. A. E. Bennett, R. G. Griffin, and S. Vega, Recoupling of homo- and heteronuclear dipolar interactions in rotating solids, *NMR Basic Principles Prog.* **12,** 1–77 (1994).
25. M. Tomaselli, B. H. Meier, M. Baldus, J. Eisenegger, and R. R. Ernst, An rf-driven nuclear spin-diffusion experiment using zero-angle sample spinning, *Chem. Phys. Lett.* **225,** 131–139 (1994).
26. T. Karlsson, M. Helmle, N. D. Kurur, and M. H. Levitt, Rotational resonance echoes in the nuclear magnetic resonance of spinning solids, *Chem. Phys. Lett.* **247,** 534–540 (1995).
27. B.-Q. Sun, P. R. Costa, D. Kocisko, P. T. Lansbury, Jr., and P. T. Griffin, Internuclear distance measurements in solid state nuclear magnetic resonance: Dipolar recoupling via rotor synchronized spin locking, *J. Chem. Phys.* **102,** 702–707 (1995).
28. P. Robyr, M. Tomaselli, J. Straka, C. Grob-Pisano, U. W. Suter, B. H. Meier, and R. R. Ernst, RF-driven and proton-driven NMR polarization transfer for investigating local order. An application to solid polymers, *Mol. Phys.* **84,** 995–1020 (1995).
29. D. M. Gregory, D. J. Mitchell, J. A. Stringer, S. Kiihne, J. C. Shiels, J. Callahan, M. A. Mehta, and G. P. Drobny, Windowless dipolar recoupling: the detection of weak dipolar coupling between spin 1/2 nuclei with large chemical shift anisotropies, *Chem. Phys. Lett.* **246,** 654–663 (1995).
30. C. A. Klug and J. Schaefer, Extension of CEDRA to homonuclear coherence transfer, *J. Magn. Reson. A* **122,** 251–253 (1996).
31. M. Eden, Y. K. Lee, and M. H. Levitt, Efficient simulation of periodic problems in NMR. Application to decoupling and rotational resonance, *J. Magn. Reson. A* **120,** 56–71 (1996).
32. M. Tomaselli, S. Hediger, D. Suter, and R. R. Ernst, Nuclear magnetic resonance polarization and coherence echoes in static and rotating solids, *J. Chem. Phys.* **105,** 10672–10681 (1996).
33. J. R. Sachleben, V. Frydman, and L. Frydman, Dipolar determinations in solids by relaxation-assisted NMR recoupling, *J. Am. Chem. Soc.* **118,** 9786–9787 (1996).
34. T. Karlsson and M. H. Levitt, Longitudinal rotational resonance echoes in solid state nuclear magnetic resonance: Investigation of zero quantum spin dynamics, *J. Chem. Phys.* **109,** 5493–5507 (1998).
35. M. Eden and M. H. Levitt, Excitation of carbon-13 triple quantum coherence in magic-angle-spinning NMR, *Chem. Phys. Lett.* **293,** 173–179 (1998).
36. M. Hohwy, H. J. Jakobsen, M. Eden, M. H. Levitt, and N. C. Nielsen, Broadband dipolar recoupling in the nuclear magnetic resonance of rotating solids: A compensated C7 pulse sequence, *J. Chem. Phys.* **108,** 2686–2694 (1998).
37. S. Kiihne, M. A. Mehta, J. A. Stringer, D. M. Gregory, J. C. Shiels, and G. P. Drobny, Distance measurements by dipolar recoupling two-dimensional solid-state NMR, *J. Phys. Chem. A* **102,** 2274–2282 (1998).
38. E. M. Menger, S. Vega, and R. G. Griffin, Observation of carbon–carbon connectivities in rotating solids, *J. Am. Chem. Soc.* **108,** 2215–2218 (1986).
39. J. M. Griffiths, K. V. Lakshmi, A. E. Bennett, J. Raap, C. M. van der Wielen, J. Lugtenburg, J. Herzfeld, and R. G. Griffin, Dipolar correlation NMR spectroscopy of a membrane protein, *J. Am. Chem. Soc.* **116,** 10178–10181 (1994).
40. T. Fujiwara, K. Sugase, M. Kainosho, A. Ono, and H. Akutsu, C-13–C-13 and C-13–N-15 dipolar correlation NMR of uniformly labeled organic-solids for the complete assignment of their C-13 and N-15 signals—An application to adenosine, *J. Am. Chem. Soc.* **117,** 11351–11352 (1995).
41. S. O. Smith, K. Aschheim, and M. Groesbeek, Magic angle spinning NMR spectroscopy of membrane proteins, *Q. Rev. Biophys.* **29,** 395–559 (1996).
42. D. Sandstrom and M. H. Levitt, Structure and molecular ordering of a nematic liquid crystal studied by natural-abundance double-quantum 13C NMR, *J. Am. Chem. Soc.* **118,** 6966–6974 (1996).
43. D. P. Weliky and R. Tycko, Determination of peptide conformations by two-dimensional magic angle spinning NMR exchange spectroscopy with rotor synchronization, *J. Am. Chem. Soc.* **118,** 8487–8488 (1996).
44. R. Tycko, D. P. Weliky, and A. E. Berger, Investigation of molecular

structure in solids by two-dimensional NMR exchange spectroscopy with magic angle spinning, *J. Chem. Phys.* **105,** 7915–7930 (1996).

45. R. Tycko, Prospects for resonance assignments in multidimensional solid-state NMR spectra of uniformly labeled proteins, *J. Biomol. NMR* **8,** 239–251 (1996).

46. P. R. Costa, J. D. Gross, M. Hong, and R. G. Griffin, Solid-state NMR measurement of Psi in peptides: A NCCN 2Q-heteronuclear local field experiment, *Chem. Phys. Lett.* **280,** 95–103 (1997).

47. M. Hong, J. D. Gross, C. M. Rienstra, R. G. Griffin, K. K. Kumashiro, and K. Schmidt-Rohr, Coupling amplification in 2D MAS NMR and its application to torsion angle determination in peptides, *J. Magn. Reson.* **129,** 85–92 (1997).

48. B. Q. Sun, C. M. Rienstra, P. R. Costra, J. R. Williams, and R. G. Griffin, 3D ^{15}N–^{13}C–^{13}C chemical shift correlation spectroscopy in rotating solids, *J. Am. Chem. Soc.* **119,** 8540–8546 (1997).

49. T. Fujiwara, T. Shimomura, and H. Akutsu, Multidimensional solid-state nuclear magnetic resonance for correlating anisotropic interactions under magic-angle spinning conditions, *J. Magn. Reson.* **124,** 147–153 (1997).

50. X. Feng, P. J. E. Verdegem, Y. K. Lee, D. Sandstrom, M. Eden, P. BoveeGeurts, W. J. deGrip, J. Lugtenburg, H. J. M. deGroot, and M. H. Levitt, Direct determination of a molecular torsional angle in the membrane protein rhodopsin by solid-state NMR, *J. Am. Chem. Soc.* **119,** 6853–6857 (1997).

51. D. A. Middleton, R. Robins, X. L. Feng, M. H. Levitt, I. D. Spiers, C. H. Schwalbe, D. G. Reid, and A. Watts, The conformation of an inhibitor bound to the gastric proton pump, *FEBS Lett.* **410,** 269–274 (1997).

52. A. E. Bennett, D. P. Weliky, and R. Tycko, Quantitative conformational measurements in solid state NMR by constant-time homonuclear dipolar recoupling, *J. Am. Chem. Soc.* **120,** 4897–4898 (1998).

53. T. Fujiwara, T. Shimomura, Y. Ohigashi, and H. Akutsu, Multidimensional solid-state nuclear magnetic resonance for determining the dihedral angle from the correlation of C-13–H-1 and C-13–C-13 dipolar interactions under magic-angle spinning conditions, *J. Chem. Phys.* **109,** 2380–2393 (1998).

54. H. W. Long and R. Tycko, Biopolymer conformational distributions from solid-state NMR: Alpha-helix and 3(10)-helix contents of a helical peptide, *J. Am. Chem. Soc.* **120,** 7039–7048 (1998).

55. M. Mehring, "Principles of High Resolution NMR in Solids," Springer-Verlag, New York (1983).

56. C. R. Sanders, B. J. Hare, K. P. Howard, and J. H. Prestegard, Magnetically-oriented phospholipid micelles as a tool for the study of membrane-associated molecules, *Prog. NMR Spectrosc.* **26,** 421–444 (1993).

57. T. A. Cross and S. J. Opella, Solid-state NMR structural studies of peptides and proteins in membranes, *Curr. Opin. Struct. Biol.* **4,** 574–581 (1994).

58. A. Ramamoorthy, F. M. Marassi, and S. J. Opella, Applications of multi-dimensional solid-state NMR spectrosocpy to membrane proteins, *in* "Proceedings of the International School of Biological Magnetic Resonance, Second Course, Dynamics and the Problem of Recognition in Biological Macromolecules" (O. Jardetsky and J. Lefeure, Eds.), pp. 237–255, Plenum Press, New York (1996).

59. C. R. Sanders and R. S. Prosser, Bicelles: A model membrane system for all seasons, *Structure* **6,** 1227–1234 (1998).

60. M. Ottiger and A. Bax, Determination of relative N–H–N N–C′, C-alpha–C′, and C(alpha)–H-alpha effective bond lengths in a protein by NMR in a dilute liquid crystalline phase, *J. Am. Chem. Soc.* **120,** 12334–12341 (1998).

61. M. Ottiger and A. Bax, Characterization of magnetically oriented phospholipid micelles for measurement of dipolar couplings in macromolecules, *J. Biomol. NMR* **12,** 361–372 (1998).